JOURNAL OF CATALYSIS 116, 95–107 (1989)

Chemical Nature of Alkali-Promoted Copper–Cobalt–Chromium Oxide Higher Alcohol Catalysts

GORDON R. SHEFFER, ROBERT A. JACOBSON,* AND TERRY S. KING[1]

*Department of Chemical Engineering and *Department of Chemistry, Iowa State University, Ames, Iowa 50011*

Received February 29, 1988; revised October 11, 1988

The chemical nature of alkali-promoted copper–cobalt–chromium higher alcohol catalysts has been evaluated as a function of calcination temperature by using X-ray diffraction and X-ray photoelectron spectroscopy. Also investigated were the alkali-promoted mono- and bimetallic oxide systems. The activated catalyst was determined to consist of copper metal and a cobalt–chromium spinel. Oxygenate production correlated with the dispersion of copper metal in the catalyst. Poorer copper dispersion and a decrease in oxygenate formation were observed with increasing catalyst calcination temperature. There was no evidence of cuprous ions or cobalt metal in the activated catalyst; therefore, it is unlikely that component synergism is a result of alkyl chain growth on cobalt metal sites coupled with alcohol termination by CO molecularly adsorbed on copper(I) chromite.

INTRODUCTION

Alkali-promoted copper–cobalt–chromium oxide catalysts are known to convert synthesis gas in high yields to normal alcohols (*1–3*). The oxygenate selectivity has been reported to exceed 95 wt%, of which 25 to 60 wt% consists of higher alcohols. The product distribution follows a Flory distribution, indicating that the catalysts resemble Fischer–Tropsch synthesis catalysts rather than alkali-promoted methanol synthesis catalysts (*4, 5*).

Because of the unique catalytic behavior and composition of these catalysts, they offer an opportunity to investigate catalyst component synergism. It is known that cobalt catalysts are very active for the Fischer–Tropsch synthesis (*6, 7*). Copper oxide (*8*) and chromium oxide are inactive for carbon monoxide hydrogenation. Copper–chromium oxide, however, is a selective methanol catalyst (*9*). In addition, a potassium-promoted copper–chromium oxide catalyst of molar composition Cu : Cr : K = 1 : 4 : 2 has been reported to produce up to 35% isobutanol at 763 K and 180 bar (1 bar = 100 kPa) (*10, 11*). However, this behavior is more comparable to that of alkali copper–zinc oxide catalysts (*4, 5*) than to the system of interest here.

From the above information one might speculate that component synergism in the copper–cobalt–chromium oxide system is a result of interaction between cobalt and copper–chromium oxide. Cobalt would provide alkyl chain growth, while copper–chromium oxide would be responsible for chain termination as alcohols. However, catalysts prepared by impregnating copper–chromium (*12*) or copper–zinc oxide (*13, 14*) methanol catalysts with cobalt or iron have not been successful in synthesizing higher alcohols.

Very little information regarding the chemical nature of the copper–cobalt–chromium oxide catalyst has been published, and consequently, little is known about the nature of the component synergism responsible for higher alcohol synthesis. Courty and co-workers (*2, 15*) have reported that calcined copper–cobalt–chro-

[1] To whom correspondence should be addressed.

0021-9517/89 $3.00

mium or aluminum–oxide catalysts consist of cupric oxide and a spinel mixed-metal oxide. Hino *et al.* (*16*) have reported similar results. Both research groups concluded from scanning transmission electron microscopy with X-ray emission microanalysis (STEM–XEM) observations that the spinel was homogeneous and not a mixture of different spinel phases. Using temperature-programmed reduction (TPR), both groups also concluded that, under typical reduction conditions, copper in the calcined catalyst was reduced to copper metal and Co^{3+} species were reduced to Co^{2+}. Steady-state catalysts were also examined by Courty and co-workers by using STEM–XEM. They found that the spinel phase was strongly depleted in cobalt and observed the formation of highly divided (1 to 3 nm) Cu–Co clusters. Although their TPR results indicate otherwise, both Courty and coworkers and Hino *et al.* speculated that copper(I) species were stabilized in the spinel or as copper chromite. These species were proposed to be responsible for the molecular adsorption of CO under reaction conditions. Metallic cobalt, thought to be formed during catalyst start-up, would be responsible for the dissociative adsorption of CO and the formation of C–C bonds. Higher alcohol synthesis was hypothesized to occur in a manner previously discussed. There is, however, little evidence to support this view of component synergism in the copper–cobalt–chromium system.

Our previous work with this catalyst has shown that calcination temperature is an important parameter in determining the oxygenate yield (*3*). Increasing the calcination temperature from 623 to 1148 K decreased the oxygenate synthesis rate from 1.6 to 0.4 μmol/m^2/min. The rate of hydrocarbon synthesis was approximately constant. These results suggested that by increasing the calcination temperature, active sites for alcohol synthesis were lost but not necessarily converted to hydrocarbon producing sites. Elucidation of the chemical nature of the copper–cobalt–chromium system as a function of calcination temperature should therefore provide valuable insight into the nature of the component synergism.

In this paper, we report the results of our study of the chemical nature of the alkali-promoted copper–cobalt–chromium catalyst as a function of calcination temperature. The study used X-ray diffraction (XRD) and X-ray photoelectron spectroscopy (XPS). The goal of this work was to correlate oxygenate selectivity and activity with the phase(s) found by catalyst characterization. In addition, we investigated the alkali-promoted mono- and bimetallic oxide systems. The nature of the component synergism operable in the copper–cobalt–chromium oxide system is discussed on the basis of the detailed characterization outlined above.

METHODS

Catalysts were prepared via homogeneous citrate complexes by using methods outlined previously (*3*). The calcined copper–cobalt–chromium catalyst samples were all prepared from the same catalyst precursor, thus eliminating any chemical differences resulting from precursor preparation. For the mono- and bimetallic oxide preparations, the molar ratio of potassium ions to transition metal ions was maintained at 0.032, the same as the ternary metal catalyst system. Cobaltous acetate, cupric nitrate, chromium trioxide, and potassium nitrate were used as metal precursors. Molar compositions of the calcined catalysts were confirmed by use of atomic absorption and flame emission spectroscopies.

Surface areas were calculated from multipoint BET adsorption isotherms of nitrogen or krypton at 77 K. Krypton was used as the adsorbate when surface areas were less than 5 m^2/g.

The catalytic behavior of all catalysts was determined in a single pass, fixed-bed, flow microreactor system described elsewhere (*17*). Before synthesis gas exposure, all catalysts were exposed to a 10% H_2 in

argon gas mixture at 548 K for 5 hr. A feed gas consisting of 58% H_2, 28% CO, and 14% Ar was used at a gas hourly space velocity of 4000 hr^{-1}. All studies were performed at 5 MPa and 548 K. By diluting the more active catalysts with α-SiO_2, the conversion of carbon monoxide was maintained at less than 10 mol% in all runs, thus minimizing heat and mass transfer limitations. Mixtures of hydrocarbons, alcohols, and aldehydes, all exclusively normal, were produced. In cases where C_2 and higher compounds were formed, product distributions were consistent with the Flory equation and chain growth probability factors (α) were determined.

Powder X-ray diffraction patterns were obtained with a Picker theta–theta diffractometer using Mo$K\alpha$ radiation. α-SiO_2 was mixed with all samples at a concentration of 5 wt% as an internal standard. The *d*-spacing of the (101) reflection was referenced to 3.342 Å. Reduced and synthesis-gas-exposed catalyst diffraction patterns were collected with a specially designed cell and procedures previously described (*17*).

X-ray photoelectron spectra were obtained with an AEI 200B spectrometer using Al$K\alpha$ radiation. Samples were prepared by loading the catalysts into soda-lime glass tubing, performing the appropriate gas treatment, and then evacuating and sealing the tubes. The tubes were transported to and opened in a helium dry box attached directly to the spectrometer. The carbon 1*s* peak resulting from adventitious carbon was reference to 285.0 eV for binding energy calculations.

RESULTS

X-Ray Diffraction

The copper–cobalt–chromium catalyst precursor was found to be amorphous. For the calcined catalysts, cupric oxide and a spinel structure (a_0 = 8.251 Å) were the only phases identified at all calcination temperatures. In addition, two other observations were made from analysis of the powder X-ray diffraction patterns for the calcined catalyst series. First, no change in the unit cell size of the spinel or cupric oxide was observed. Second, the amount of cupric oxide relative to the spinel phase was found to increase with increasing calcination temperature.

The *d*-spacings of the spinel and cupric oxide reflections are given in Table 1. Only those reflections which occur with minimum overlap of the two phases are listed. The *d*-spacings for cupric oxide agree well with those in the literature (*18*). While a variety of copper, cobalt, and/or chromium spinels have been reported in the literature (see Table 2), it is not possible to identify the composition of the spinel found in this study by simple comparison of unit cell sizes because, as will be discussed later, there are numerous spinels with variable composition that can have identical cell sizes.

To quantify the relative amounts of each phase present, the integrated area of the (202) cupric oxide peak was normalized with respect to the (400), (220), and (111) peaks of the spinel. These peaks were chosen because of the absence of overlap with other peaks in the spectrum. The ratio of the cupric oxide area to the spinel area as a function of calcination temperature is provided in Table 1. A factor of three increase in the amount of cupric oxide visible in the diffraction pattern relative to the amount of spinel was observed.

X-ray diffraction of synthesis-gas-exposed catalysts indicated that the cupric oxide reduced completely to copper metal. The spinel phase was slightly affected as evidenced by the small shift of the *d*-spacings (see Table 3). No additional phases were detected. Comparison of the copper metal peak areas to the spinel peak areas as was done for the calcined catalysts revealed little variation among the samples, indicating that all the copper in the catalyst was now visible to XRD. However, the copper metal peak width decreased monotonically from the catalyst that had been

TABLE 1

d-Spacings of Spinel and Cupric Oxide Reflections and Peak Area Ratio of Cupric Oxide to Spinel as a Function of Catalyst Calcination Temperature

Calcination temperature (K)	Spinel *d*-spacings (Å)			CuO *d*-spacings (Å)			Area ratio CuO/spinel
	(440)	(533)	(731)	(111)	(202)	(113)	
623	1.460	1.258	1.077	2.330	1.876	1.504	0.33
798	1.460	1.261	1.079	2.325	1.869	1.502	0.73
973	1.458	1.259	1.073	2.330	1.867	1.509	0.89
1148	1.457	1.258	1.075	2.326	1.869	1.507	1.00

calcined at 623 K to the catalyst that had been calcined at 1148 K. Mean copper metal particle sizes (see Table 3) were calculated from the peak width of the Cu(111) reflection using the Scherrer equation (*21*)

$$\bar{d} = 0.89\lambda_{Mo}/\cos\theta/(w_s - w_i)^{1/2},$$

where $\bar{d}$ is the mean crystallite particle diameter, λ_{Mo} the wavelength for molybdenum radiation, θ the Bragg angle, w_s the peak width at half-height of the Cu(111) reflection, and w_i the instrumental peak width correction factor.

When reduced catalysts were exposed to air, heat generation occurred, indicating sample reoxidation. The powder diffraction patterns of the reoxidized catalysts indicated that a portion of the copper metal was oxidized to cupric and cuprous oxide. As qualitatively observed in Fig. 1, the amount of copper reoxidized decreased with increasing calcination temperature of the catalyst. The *d*-spacings of the spinel after catalyst reoxidation were the same as those observed for the synthesis-gas-treated catalysts (see Table 3) obtained under controlled atmosphere.

TABLE 2

Lattice Parameters of Copper–Cobalt–Chromium Spinels

Spinel	Lattice parameter a_0 (Å)	Reference
$Cu(II)Cr(III)_2O_4$	8.344	—[a]
$Co(II)Cr(III)_2O_4$	8.333	19
$Co(II)Co(III)Cr(III)O_4$	8.209	19
$Cu(II)Co(III)_2O_4$	8.084	20
$Co(II)Co(III)_2O_4$	8.084	19

[a] Joint Committee on Powder Diffraction Standards #26-508.

X-Ray Photoelectron Spectroscopy

X-ray photoelectron spectroscopy results for the samples prepared at the lowest and highest calcination temperatures are summarized in Table 4. Results are reported for catalysts after calcination, reduction, and synthesis gas exposure. Catalysts prepared at intermediate calcination temperatures had similar results.

Potassium exhibits very little chemical shift, so that no information concerning its chemical state can be deduced. The intensity of the potassium signal was observed to be very strong. Since only a minor amount of potassium was incorporated into the catalysts, the strength of the signal indicates that the catalyst surfaces are enriched in potassium. The citrate complexation method is known to cause the formation of potassium carbonate (*17*). However, inspection of the C-1*s* spectra for these catalysts revealed no carbonate formation in the copper–cobalt–chromium catalyst system. In addition, inspection of the C-1*s* spectra of calcined or synthesis-gas-exposed catalysts provided no evidence of any metal carbide formation.

The chromium binding energies given in Table 4 are typical of Cr^{3+} species (*22*).

TABLE 3

d-Spacings of Spinel and Copper Metal Reflections and Mean Copper Metal Particle Diameter in Synthesis-Gas-Exposed Catalysts as a Function of Calcination Temperature

Calcination temperature (K)	Spinel *d*-spacings (Å)			Copper metal *d*-spacings (Å)		Mean copper particle diameter (nm)
	(440)	(533)	(731)	(111)	(200)	
623	1.466	1.264	1.080	2.085	1.809	9.5
798	1.464	1.263	1.079	2.089	1.812	12.4
973	1.466	1.268	1.082	2.089	1.811	17.6
1148	1.466	1.268	1.082	2.089	1.811	22.9

Chromium trioxide, the metal salt used to form the catalyst precursor, is a strong oxidizer, and the reduction of Cr^{6+} to Cr^{3+} was not unexpected. Although chromium(III) oxides are reducible (*23*), no change in the chromium $2p_{3/2}$ position or peak shape was observed upon hydrogen or synthesis gas exposure; no change would suggest no further chromium reduction at these conditions.

The cobalt binding energies listed in Table 4 are typical of Co^{2+} or Co^{3+} species (*22*). The difference in binding energies of Co^{2+}/Co^{3+} species in mixed cobalt oxide compounds, such as spinels, is not great enough to allow differentiation of the two species. No change in peak position was observed for the reduced and synthesis-gas-exposed samples. Also, no peak or shoulder at lower binding energies that could be assigned to fully reduced cobalt species was observed. However, the intensity of the Co-$2p_{1/2}$ and Co-$2p_{3/2}$ satellite peaks was found to be much greater for the reduced and synthesis-gas-exposed samples. Frost *et al.* (*24*) have observed similar intense satellite peaks for high-spin Co^{2+} ions, while diamagnetic Co^{3+} and low-spin Co^{2+} ions had much less intense satellites.

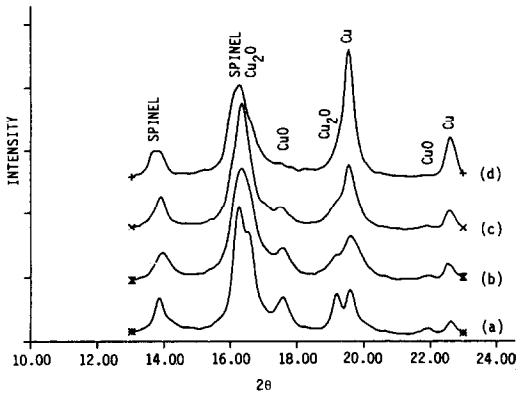

FIG. 1. Powder X-ray diffraction patterns of calcined catalysts after reduction and exposure to air. (a) calcined at 623 K, (b) calcined at 798 K, (c) calcined at 973 K, and (d) calcined at 1148 K.

In order to evaluate the three oxidation states of copper (0, 1+, 2+), both the core-emitted photoelectrons and the X-ray-induced Auger transitions must be examined. Cu^{2+} can be distinguished from Cu^0 and Cu^{1+} species by the Cu-$2p_{3/2}$ binding energies. Cu^{2+} species have a binding energy of approximately 933.5 eV, while Cu^0 and Cu^{1+} species have a binding energy of approximately 932.2 eV (*22, 25*). In addition the Cu-$2p_{3/2}$ spectrum of Cu^{2+} species contains satellite peaks due to shake-up processes. To distinguish the Cu^0 and Cu^+ oxidation states, analysis of the X-ray-induced Auger transitions must be included. Specifically, the Auger parameter, β, is calculated. β is defined by

$$\beta = KE_{2p_{3/2}} - KE_{LMM},$$

where $KE_{2p_{3/2}}$ is the kinetic energy of the Cu-$2p_{3/2}$ photoelectron line and KE_{LMM} is the kinetic energy of the Cu-$L_3,M_{4,5}M_{4,5}$ Auger transition. One advantage of the Au-

TABLE 4

X-Ray Photoelectron Spectroscopy Results

Calcination temperature (K)	Treatment	Binding energies (eV)				
		K($2p_{3/2}$)	Cr($2p_{3/2}$)	Co($2p_{3/2}$)	Cu($2p_{3/2}$)	Cu($\beta + h\nu$)
673	Calcined	293.0	576.1	780.1	933.8	1851.4
	Reduced	293.0	575.9	779.9	932.0	1851.3
	Syn-gas	293.1	576.2	780.3	932.0	1851.1
1148	Calcined	293.0	576.0	779.9	933.7	1851.4
	Reduced	293.0	576.0	780.0	931.9	1851.3
	Syn-gas	293.2	576.4	780.0	932.2	1851.1

ger parameter is that sample charging effects subtract out. In general, Auger parameters are tabulated as $\beta + h\nu$, where $h\nu$ is the energy of the excitation source. The value is then independent of the excitation source. Cu^+ species have $\beta + h\nu$ values of 1849.4 ± 0.4 eV, while Cu^0 and Cu^{2+} species have values of 1851.2 ± 0.4 eV.

For the catalysts in this study, the data in Table 4 show that the copper in the calcined catalysts was present as Cu^{2+}. A strong satellite structure was also observed in the calcined catalyst spectra. Upon hydrogen and synthesis gas exposure, the copper was fully reduced to copper metal. Examination of the Auger transition region provided no evidence of any Cu^+ species.

Mono- and Bimetallic Catalysts

Reactor studies. The molar composition and the surface areas of the mono- and bimetallic catalysts both after calcination and after synthesis gas reaction are presented in Table 5. As is commonly observed (*4, 17*), the addition of potassium increased the degree of sintering upon reduction. Catalysts containing chromium had larger surface areas than those containing copper and cobalt alone or mixed.

The catalytic behavior of these catalysts is summarized and compared to that for the copper–cobalt–chromium system in Table 5. As mentioned earlier, unpromoted cobalt is a very active Fischer–Tropsch catalyst. Our results indicated that the activity or selectivity of cobalt was not altered by using the citrate complexation method of preparation. When potassium was introduced, three changes in catalytic behavior were noted. First, the activity decreased by a factor of 5. Second, oxygenates were produced with modest (~40 wt%) selectivity. Third, the average molecular weight of the product decreased, as reflected by the 37% decrease in α with potassium promotion of cobalt. A comparable decrease in activity has been observed by Fujimoto and Oba (*26*) for a potassium-promoted, silica-supported cobalt catalyst under similar reaction conditions. However, their data indicate only a small increase, from 10 to 20 wt%, in oxygenate selectivity. The 37% decrease in α observed in our study was unexpected. Other studies of the influence of potassium on Fischer–Tropsch cobalt/kieselguhr catalysts found that potassium had little influence on the product selectivity, unlike iron catalysts, where α increased with potassium promotion (*6*). It is possible that potassium simply blocks cobalt sites at the surface; this blocking would decrease activity and increase the separation of cobalt sites. Bartholomew and Reuel (*27*) have reported both a decrease in activity and a decrease in the average chain length of the hydrocarbon product with increasing dispersion for unpromoted, supported cobalt catalysts. Only a small increase in oxygenate selectivity was noted. However, their study was conducted at atmospheric

TABLE 5

Catalytic Behavior of Mono- and Bimetallic Catalysts[a]

Catalyst[b]	Surface area (m^2/g)		Activity μmol CO/ m^2 min	Selectivity (wt%)[d,e,f] product distribution (α)		
	Calcined	Used		HYD	ALC	ALD
Co	—[c]	2.4	900	100 (α = 0.67)	—	—
$CoK_{0.032}$	2.2	0.6	184	60 (α = 0.46)	11 (α = 0.39)	29 (α = 0.36)
Cu	—[c]	2.3	<0.4	75	25	—
$CuK_{0.032}$	1.8	0.8	36	5	95	—
$CrK_{0.032}$	28.3	29.1	0.03	100	—	—
$CoCuK_{0.064}$	1.3	0.8	23	54 (α = 0.34)	28 (α = 0.11)	18 (α = 0.32)
$CoCrK_{0.064}$	59.4	65.9	0.7	100 (α = 0.60)	0	0
$CuCrK_{0.064}$	16.0	14.8	7.0	1	99	0
$CuCoCr_{0.8}K_{0.092}$	29.0	28.7	5.8	33 (α = 0.46)	58 (α = 0.43)	9

[a] Steady state, T = 548 K, P = 5 MPa, H_2/CO = 2.
[b] Molar composition.
[c] Not measured.
[d] Excluding H_2O and CO_2.
[e] HYD, hydrocarbons; ALC, alcohols; ALD, aldehydes.
[f] Absence of an α value indicates that only the C_1 product was produced.

pressure, and in general, the formation of oxygenates from synthesis gas requires 3 to 10 MPa pressure.

In agreement with other researchers (*7, 8, 28*), our study found unpromoted copper catalysts to be inactive for carbon monoxide hydrogenation. Surprisingly, the incorporation of potassium resulted in a very active and selective methanol catalyst. Details concerning the promotional effect of potassium on copper may be found elsewhere (*17*). Briefly, potassium was found to stabilize the formation of Cu^+ species that have been implicated as active sites for methanol synthesis in other catalytic systems under reaction conditions.

The preparation of a catalyst containing both copper and cobalt yielded a catalyst with characteristics of the individual components; that is, methanol and a hydrocarbon/aldehyde mixture were produced. The decrease in activity compared to alkali-promoted cobalt or copper alone indicated that some interaction between copper and cobalt must be occurring. A 26% decrease in the hydrocarbon chain growth parameter was also observed. Similar decreases in activity and in the average molecular weight of the product have been reported for copper introduction onto supported ruthenium Fischer–Tropsch catalysts (*29, 30*).

A potassium-promoted copper–chromium catalyst resulted in an active and selective methanol catalyst. No higher alcohols were observed. However, the levels of potassium promotion, temperature, and pressure used in our study are all much less than those used in the work of Tahara, discussed earlier (*10, 11*). The methanol synthesis rate of the potassium-promoted copper–chromium catalyst is a factor of 5 greater than that reported for an unpro-

moted catalyst with a copper-to-chromium molar ratio of unity (*31*). Since our study has found that copper promoted by potassium can produce methanol, the increase in rate may be attributable to this interaction.

The cobalt–chromium oxide catalyst exhibited very low activity and was selective to hydrocarbons. This is in agreement with recent work by Fornasari *et al.* (*32*) with cobalt–chromium oxide catalysts. The similarity of the product distribution of cobalt metal with the cobalt–chromium catalyst suggests that a small amount of segregated cobalt metal is responsible for what little catalytic activity is found in our study.

X-Ray diffraction. The powder X-ray diffraction results for calcined and reduced, potassium-promoted catalyst samples are summarized in Table 6. No potassium phases were observed in any of the diffraction patterns. This is to be expected when the low concentrations of potassium used are considered.

For the monometallic catalysts, both cobalt oxide and copper oxide fully reduce to the metals. Cobalt metal forms a mixture of the face-centered cubic form and the hexagonal form (α-Co) as has been observed by Hofer and Peebles (*33*). As was observed in the copper–cobalt–chromium catalyst system, chromium(III) oxide did not reduce at the reduction temperatures used in this study.

The cobalt–copper oxide catalyst precursor formed a mixture of the cobalt and copper oxides upon calcination. Cobalt oxide is known to dissolve up to 25 mol% CuO with no change in the cell parameters (*34*); therefore, mixing of the two phases in the calcined catalyst may have occurred. There was no evidence for the formation of cobalt–copper spinels. These spinels are very sensitive to preparation procedures (*20*) and apparently do not form by using the citrate complexation method of preparation. Upon reduction total phase segregation into Co and Cu metal was observed. Cobalt and copper metal have an extremely limited miscibility region (*35*) and hence alloy formation is not expected.

The copper–chromium catalyst contained a variety of phases. The reduced catalyst was primarily Cu metal and $CuCrO_2$. The presence of $CuCrO_2$ agrees with previous work (*31*) where $CuCrO_2$ was shown to be the active phase for methanol synthesis.

The cobalt–chromium catalyst was observed to form a spinel with an equimolar ratio of the two metals. The stability of both the 2+ and 3+ oxidation states for cobalt allows for the formation of a variety of cobalt–chromium spinels ranging in composition from $CoCr_2O_4$ to Co_2CrO_4. In these spinels, octahedral Co^{3+} ions are reported to be in a low-spin (diamagnetic) state while tetrahedral Co^{2+} ions are in a high-spin state. In Table 7 the *d*-spacings of the re-

TABLE 6

X-Ray Diffraction Results for Potassium-Promoted Mono- and Bimetallic Catalyst Systems

Catalyst	Calcined phase(s)		Reduced phase(s)	
	Major	Minor	Major	Minor
$CoK_{0.032}$	Co_3O_4	CoO	Co, α-Co	—
$CuK_{0.032}$	CuO	—	Cu	—
$CrK_{0.032}$	Cr_2O_3	—	Cr_2O_3	—
$CoCuK_{0.064}$	CoO, CuO	Co_3O_4	Co, Cu	α-Co
$CoCrK_{0.064}$	$Co_{1.5}Cr_{1.5}O_4$	—	$Co_{1.5}Cr_{1.5}O_4$	—
$CuCrK_{0.064}$	CuO, $CuCr_2O_4$	Cr_2O_3, $CuCrO_2$	$CuCrO_2$, Cu	Cr_2O_3, $CuCr_2O_4$

TABLE 7

d-Spacings for Cobalt–Chromium Spinels

Spinel composition	*d*-Spacing (Å)						Reference
	(311)	(400)	(511)	(440)	(533)	(731)	
$CoCr_2O_4$	2.512	2.083	1.604	1.473	1.271	1.085	19
$Co_{1.5}Cr_{1.5}O_4$	2.493	2.067	1.592	1.462	1.261	1.077	Average[a]
Co_2CrO_4	2.475	2.052	1.580	1.451	1.252	1.069	19
Calcined catalyst[b]	2.488	2.064	1.589	1.458	1.259	1.074	This work
Reduced catalyst[b]	2.489	2.065	1.592	1.461	1.260	1.077	This work

[a] On the basis of linearity of unit cell sizes (*19*).
[b] Composition: $Co_{1.5}Cr_{1.5}K_{0.064}$.

flection planes for the spinel formed in this study are compared to other cobalt–chromium spinel compositions. The *d*-spacings for $Co_{1.5}Cr_{1.5}O_4$ were calculated by averaging the values of the *d*-spacings for $CoCr_2O_4$ and Co_2CrO_4. The use of a linear relationship to calculate the change in *d*-spacings with increasing cobalt content has been shown to be valid by Bracconi *et al.* (*19*). The agreement between the calculated and the experimentally determined *d*-spacings for the equimolar cobalt–chromium spinel is excellent, indicating that the citrate complexation preparation method yields a very homogeneous spinel. In agreement with the study of Fornasari *et al.* (*32*), the spinel was stable under a reducing atmosphere as evidenced by no change in the *d*-spacings and no observation of additional phases in the diffraction pattern.

DISCUSSION

The powder X-ray diffraction patterns of the calcined copper–cobalt–chromium catalysts indicated the presence of a spinel compound and cupric oxide. This is consistent with the results of Courty and co-workers (*2, 15*) and of Hino *et al.* (*16*) presented earlier. The composition of the spinel is difficult to determine from X-ray diffraction results alone, because as evidenced from the data in Table 2, the replacement of Co^{2+} ions by Cu^{2+} ions on tetrahedral sites in the spinel has little or no effect on the lattice parameter. Consequently, the diffraction pattern of $CuCoCrO_4$, for example, would be identical to that for Co_2CrO_4. However, the composition of the octahedral positions (Cr^{3+} or Co^{3+}) does influence the unit cell size as shown in Table 7. Comparing the *d*-spacings of the spinel found in the calcined catalysts (see Table 1) with the *d*-spacings of cobalt–chromium spinels (see Table 7), we can assign a variable composition to the catalyst spinel of

$$[Cu(II)_x(Co(II)_{1-x}][Co(III)_{0.64}Cr(III)_{1.36}]O_4,$$

where $0 \leq x \leq 1$. Note that if $x = 0$, the spinel composition is $Co_{1.64}Cr_{1.36}O_4$. The Co : Cr ratio would be 1.21, which is very close to 1.25, the Co : Cr ratio formulated into the catalyst. For $0 < x \leq 1$, a mass balance dictates that a portion of the cobalt must exist outside of the spinel. However, at all of the calcination temperatures studied, the spinel and cupric oxide were the only phases observed. The possibility of obtaining a poorly crystallized Co oxide phase at a calcination temperature of 1148 K is unlikely. Additionally, cobalt oxide has a very low solubility in cupric oxide (*20*), eliminating the possibility of cobalt being incorporated into cupric oxide and not being detected. Hence it is deduced that the spinel found in the calcined catalysts has composition $Co_{1.64}Cr_{1.36}O_4$ with no copper incorporation. The increase in the amount of cupric oxide relative to the

spinel (see Fig. 2) is interpreted as a decrease in the cupric oxide dispersion; that is, the cupric oxide becomes more visible as it forms larger particles at the expense of smaller particles.

When the catalyst is reduced and exposed to synthesis gas, two changes occur in the catalyst. First, all of the Cu^{2+} species in the calcined catalyst are reduced to copper metal. There is no evidence from either XPS or XRD of any Cu^{2+} or Cu^{+} species. Since the smallest mean copper particle diameter in the synthesis-gas-exposed catalysts is 9.5 nm (see Table 3), much larger than the approximately 2.0 nm limit necessary for a particle to be visible by X-ray diffraction, all of the copper in the sample will be observable by XRD. In this case, the XRD copper metal peak area to spinel peak area ratio would be constant, as was experimentally observed. The increase in the copper metal particle diameter in the synthesis-gas-exposed catalysts with increasing calcination temperature reflects a decrease in the dispersion of copper metal similar to that observed for cupric oxide in the calcined catalysts. The decrease in copper metal dispersion with increasing calcination temperature is also indicated by the decrease in reoxidation of copper metal upon exposure of the reduced catalysts to air. The larger copper metal particles do not reoxidize completely but form a core of metal surrounded by an oxide shell. Second, part of the cobalt undergoes reduction as indicated by the slightly larger *d*-spacings for the spinel in the synthesis-gas-exposed catalysts (see Table 3) as compared to that *d*-spacings for the calcined catalysts (see Table 1).

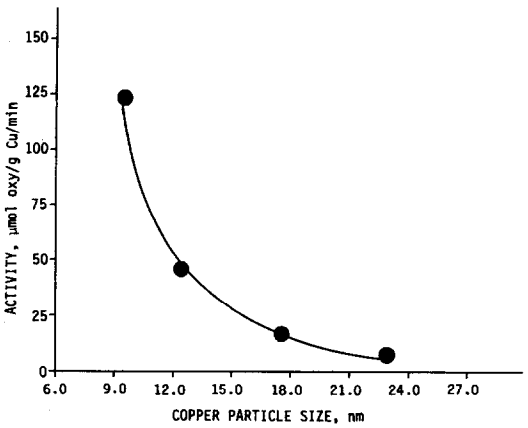

FIG. 2. Oxygenate synthesis rate as function of copper metal particle diameter in synthesis-gas-exposed catalysts.

Comparison of the diffraction lines of the synthesis-gas-exposed catalysts to those of the calcined catalyst suggests that the spinel in the calcined catalyst is reduced to $Co_{1.34}Cr_{1.66}O_4$. A mass balance indicates that approximately one-third of the cobalt in the sample is not incorporated into the spinel structure. The increase in the intensity of the cobalt satellite peaks in the X-ray photoelectron spectra is evidence of the reduction of some of the Co^{3+} ions to Co^{2+}. The absence of a clearly defined shoulder or peak in the X-ray photoelectron spectra that could be assigned to cobalt metal indicates that either the cobalt present outside of the spinel is Co^{2+} or, if reduced fully, the cobalt metal formed is not in an appreciable concentration at the catalyst surface. A point of interest is that the cobalt–chromium spinel is partially reduced only upon the addition of copper to the system. A similar phenomenon is observed for Fischer–Tropsch iron catalysts, where the addition of small amounts of copper to the catalyst increases the reduction rate of iron oxide (*36*). As a results, lower reduction temperatures may be used. The overall extent of reduction of the cobalt–chromium spinel is not affected by the copper dispersion, as evidenced by the invariance of the *d*-spacings for the reduced catalysts (see Table 3).

The picture of the catalyst that evolves from the above discussion is that in the activated catalyst, copper metal is supported on a cobalt–chromium spinel. As an initial evaluation of this hypothesis, a portion of the equimolar cobalt–chromium spinel previously prepared was impregnated with cupric nitrate. The amount of cupric nitrate

used was calculated to yield two monolayers of copper metal. The overall molar composition of the resulting catalyst was $CoCrCu_{0.6}K_{0.05}$. After impregnation by incipient wetness and drying at 543 K, the catalyst was reduced in diluted hydrogen. No intermediate calcination step was used. The catalytic behavior of the catalyst is compared to that of the spinel and previous results (*3*) for a $CuCoCr_{0.8}K_{0.09}$ catalyst prepared via citrate complexation methods in Table 8. While the cobalt–chromium spinel alone did not produce oxygenates, impregnation of the spinel with copper yielded a selectivity to oxygenates of 60 wt%. Furthermore, an increase in catalytic activity is observed, indicating that copper plays an active role in the synthesis of oxygenates. This role is further emphasized if the activity data previously reported for the copper–cobalt–chromium catalyst are plotted as a function of the mean copper metal particle diameter of the synthesis-gas-exposed catalysts as found by XRD (see Fig. 2). Oxygenate synthesis is directly related to copper metal dispersion.

To be explored is the unknown nature of the component synergism responsible for oxygenate formation. Although their TPR studies indicate otherwise, both Courty *et al.* (*2*) and Hino *et al.* (*16*) have speculated that copper is only partially reduced to copper metal and that a portion of the copper is stabilized as Cu^+ through formation of a copper(I)–aluminum or copper(I)–chromium oxide. The Cu^+ phases, which are known to be active for methanol synthesis (*31*) and which have been shown to form in the copper–zinc oxide (*37*), copper–chromium oxide (*31*), and copper–potassium methanol catalyst (*17*) systems, would then be responsible for termination to alcohols of alkyl chains growing on cobalt metal clusters. Our results indicate that no evidence exists for the formation of Cu^+ or cobalt metal species at the catalyst surface. Therefore, the previously proposed view of component synergism is improbable.

Small copper–cobalt metal clusters 1 to 3 nm in diameter, such as those observed on copper–cobalt–aluminum catalysts (*2*), would most likely be inactive for carbon monoxide hydrogenation, because the activity of supported cobalt (*27*) and ruthenium (*38*) catalysts is reported to decrease with increasing dispersion. The data of Bartholomew and Reuel (*27*) indicate that cobalt on alumina is inactive at a dispersion of 17%; this corresponds to a mean particle diameter of approximately 4 nm. Similarly, Lin and Pennella (*12*) have found that cobalt impregnation of copper–zinc–alumina

TABLE 8

Comparison of Catalytic Behavior of Copper-Impregnated Cobalt–Chromium Spinel[a]

Catalyst	Preparation	Selectivity (wt%)[b,c]			Product distribution (α)				Activity μmol CO/ m^2 min
		HYD	ALC	ALD	HYD	ALC	ALD	ALL	
$Cu_{0.6}CoCrK_{0.05}$	Copper nitrate impregnation of $CoCrK_{0.064}$	40	58	2	0.47	0.36	—	0.42	1.0
$CuCoCr_{0.8}K_{0.09}$	Citrate complexation	33	58	9	0.46	0.43	—	0.43	5.8
$CoCrK_{0.064}$	Citrate complexation	100	—	—	0.60	—	—	0.60	0.4

[a] Steady state, T = 548 K, P = 5 MPa, H_2/CO = 2.
[b] Excluding H_2O and CO_2.
[c] HYD, hydrocarbons; ALC, alcohols; ALD, aldehydes; ALL, all functionalities combined.

oxide methanol catalysts simply deactivate the active sites for methanol synthesis for cobalt loadings up to approximately 1 wt%. Only when the cobalt loading was increased to greater than 1 wt% did the synthesis of hydrocarbons occur. The selectivity to higher oxygenates never exceeded 20 wt% for any of the various cobalt loadings they studied. The addition of copper to small cobalt metal clusters would depress the cobalt activity every further, as is observed for supported ruthenium–copper catalysts (*29, 30*). The alkali-promoted cobalt–copper catalyst examined in this study indicated no enhancement of higher oxygenate productivity, although interaction between copper and cobalt must have been occurring as evidenced by a decrease in activity greater than that due to averaging of the individual components. The formation of a cobalt–chromium spinel, therefore, appears necessary to obtain high oxygenate selectivity.

The modification of copper(I)–chromium oxide methanol sites by potassium is discounted by the results of this study as well since no higher alcohol formation was observed for the alkali-promoted copper–chromium catalyst. At the same time, the absence of higher oxygenate formation for the potassium-promoted copper–chromium oxide catalyst underscores the fact that cobalt appears to be a necessary component for higher oxygenate formation in the copper–cobalt–chromium oxide system.

Copper metal is known to be susceptible to electronic interactions with some supports. Chen *et al.* (*28*) found that when copper metal was supported on Cr_2O_3 or ZrO_2, which are *p*-type semiconductors, the turnover rate for carbon monoxide hydrogenation increased by an order of magnitude over that of bulk copper. The authors proposed that a very localized interaction between the copper and the support occurs at the point where the two materials are in contact. We have observed previously that unsupported copper–lithium catalysts can produce a Flory distribution of hydrocarbons and alcohols (*17*). The activity of the catalyst was 10 μmol CO/m^2/min, comparable to that for the copper–cobalt–chromium system. A distinct possibility exists that copper is electronically modified on a potassium-promoted cobalt–chromium spinel. A decrease in copper dispersion, that is, larger particles, as was observed with increasing catalyst calcination temperature, would result in a decrease in the amount of copper/spinel interaction and thus a decrease in catalytic activity. In fact, if the data in Fig. 2 are normalized to the estimated copper/spinel interfacial area rather than to the total weight of copper, then the activity does not change by more than a factor of 2 over the entire range of particle sizes. No direct evidence was obtained in our study that the electronic state of copper had indeed been altered, however. The role of oxidized cobalt species in the catalyst system may be to provide further electronic modification of the chromia or else stabilize molecularly adsorbed carbon monoxide at the copper interface (*39*).

Two questions become apparent: (i) Why does potassium promotion of the cobalt catalyst cause an increase in oxygenate production? (ii) Would not this interaction be important in the Cu–Co–Cr system? The answers may involve the presence of oxidize cobalt species. These species are speculated to be responsible for the formation of C_2 oxygenates on SiO_2 supported cobalt catalysts modified with Ru and Sr (*40*). The answers could also involve the role of potassium in a manner similar to that operable in copper–lithium catalysts (*17*). In any case, since the alkali-promoted, copper–cobalt catalyst examined in this study exhibited no increase in selectivity to higher oxygenates above that associated with potassium-promoted cobalt, it would appear that the behavior of the cobalt–copper–chromium system is not related to the interaction of potassium-promoted cobalt species with copper. Certainly more work is needed to discern the nature of the active site in greater detail and to understand the role of copper metal and cobalt–chromium

spinel in the mechanism of higher alcohol synthesis.

ACKNOWLEDGMENTS

The authors gratefully acknowledge the Shell Co. Foundation's Faculty Initiation Fund. In addition, this work was aided, in part, by a Grant-in-Aid of Research from Sigma Xi. One of the authors (G.R.S.) wishes to thank the Amoco Foundation for fellowship support. Also acknowledged with appreciation is James Anderegg (Ames Laboratory) for assistance in collection of X-ray photoelectron spectra.

REFERENCES

1. Sugier, A., and Freund, E., U.S. Patent 4,122,110 (1978).
2. Courty, P., Durnad, D., Freund, E., and Sugier, A., *J. Mol. Catal.* **17,** 241 (1982).
3. Sheffer, G. R., and King, T. S., *Appl. Catal.*, **44,** 153 (1988).
4. Smith, K. J., and Anderson, R. B., *Canad. J. Chem. Eng.* **61,** 40 (1983).
5. Smith, K. J., and Anderson, R. B., *J. Catal.* **85,** 428 (1984).
6. Anderson, R. B., *in* "Catalysis" (P. Emmett, Ed.), Vol. 4, Chap. 2. Reinhold, New York 1956.
7. Vannice, M. A., *J. Catal.* **50,** 228 (1977).
8. Klier, K., *Adv. Catal.* **31,** 243 (1982).
9. Apai, G. R., Monnier, J. R., and Hanrahan, M. J., *J. Chem. Soc. Chem. Commun.*, 212 (1984).
10. Tahara, H., Tatuki, Y., and Simizu, J., *J. Soc. Chem. Ind.* (*Japan*) **43,** 8213 (1940).
11. Tahara, H., Komiyauma, D., Kodama, S., and Ishibashi, T., *J. Soc. Chem. Ind.* (*Japan*) **45** (supplement), 89 (1942).
12. Lin, F. N., and Pennella, F., *in* "Catalytic Conversions of Synthetic Gas and Alcohols to Chemicals" (R. Herman, Ed.), pp. 53–63. Plenum, New York, 1984.
13. Elliott, D. J., and Pennella, F., *J. Catal.* **102,** 464 (1986).
14. Sibilia, J. A., Dominguez, J. M., Herman, R. G., and Klier, K., *Amer. Chem. Soc. Div. Fuel Chem. Prepr. Pap.* **29,** 226 (1984).
15. Courty, P., and Marcilly, C., *in* "Preparation of Catalysts III" (G. Poncelet, P. Grange, and P. Jacobs, Eds.), pp. 485–519. Elsevier, Amsterdam, 1983.
16. Hino, T., Nomura, T., and Kayano, T., *Sekiyu Gakkaishi* **27,** 257 (1984).
17. Sheffer, G. R., Ph.D. thesis, "Investigation of the catalytic and chemical nature of alkali promoted copper and copper–cobalt–chromium oxide catalysts for the conversion of synthesis gas to methanol and higher alcohols." Iowa State Univ., Ames, IA, 1987.
18. Joint Committee on Powder Diffraction Standards, File #4-836.
19. Bracconi, P., Bertnod, L., and Dufour, L. C., *Ann. Chim.* (*Paris*) **4,** 331 (1979).
20. Rasines, I., *J. Appl. Crystallogr.* **5,** 11 (1972).
21. Anderson, J. R., "Structure of Metallic Catalysts," pp. 365–368. Academic Press, New York, 1975.
22. "Handbook of X-ray Photoelectron Spectroscopy" (G. E. Muilenberg, Ed.). Physical Electronics, Eden Prairie, MN, 1976.
23. Tauster, S. J., Fung, S. C., Baker, R. T. K., and Horsley, J. A., *Science* **221,** 1121 (1981).
24. Frost, D. C., McDowell, C. A., and Woolsey, I. S., *Mol. Phys.* **27,** 1473 (1974).
25. McIntyre, N. S., Rummery, T. E., Cook, M. G., and Owen, D., *J. Electrochem. Soc.* **123,** 1123 (1976).
26. Fujimoto, K., and Oba, T., *Appl. Catal.* **13,** 289 (1985).
27. Bartholomew, C. H., and Reuel, R. C., *Ind. Eng. Chem. Prod. Res. Dev.* **24,** 56 (1985).
28. Chen, H-W., White, J. M., and Ekerdt, J. G., *J. Catal.* **99,** 293 (1986).
29. Bond, G. C., and Turnham, B. D., *J. Catal.* **45,** 128 (1976).
30. Lai, S. Y., and Vickerman, J. C., *J. Catal.* **90,** 337 (1984).
31. Monnier, J. R., Hanrahan, M. J., and Apai, G. R., *J. Catal.* **92,** 119 (1985).
32. Fornasari, G., Gusi, S., Trifirò, F., and Vaccari, A., *Ind. Eng. Chem. Res.* **26,** 1500 (1987).
33. Hofer, L. J. E., and Peebles, W. C., *J. Amer. Chem. Soc.* **69,** 897 (1947).
34. Delorme, C., *Bull. Soc. Fr. Mineral. Cristallogr.* **81,** 19 (1958).
35. Hultgren, R. R., Desai, P. D., Hawkins, D. T., Gleiser, M., and Kelley, K. K., "Selected Values of the Thermodynamic Properties of Binary Alloys," pp. 652–655. American Society for Metals, Metals Park, OH, 1973.
36. Roper, M., *in* "Catalysis in C_1 Chemistry" (W. Keim, Ed.), pp. 41–88. Reidel, New York, 1983.
37. Herman, R. G., Klier, K., Simmons, G. W., Finn, B. P., Bulko, J. B., and Kobylinski, T. P., *J. Catal.* **56,** 407 (1979).
38. Kellner, C. S., and Bell, A. T., *J. Catal.* **75,** 251 (1982).
39. Fierro, J. L. G., and Garcia De La Banda, J. S., *Catal. Rev. Sci. Eng.* **28,** 265 (1986).
40. Sugi, Y., Takeuchi, K., Matsuzaki, T., and Arakawa, H., *Chem. Lett.*, 1315 (1985).